

Chapter 3

AC electrooptic experiments on a hybrid aligned nematic(HAN) cell

In this chapter, we will discuss the electrooptic measurements on a hybrid aligned nematic cell. Under the influence of an externally applied field, there is a reorientation of the director in the volume of the cell. The optical properties of the medium are changed as a result of this reorientation giving rise to an electrooptical signal. The phase retardation due to the different speeds of the extraordinary rays and ordinary rays in the liquid crystalline medium determines the electrooptic response between crossed polarisers.

The **AC** and **DC** transmitted intensities of a HAN cell are measured as functions of voltage at different temperatures for a particular compound. By fitting the experimental transmitted intensity curve to the calculated intensity profiles, we are able to measure the anchoring energies at both the surfaces of a **HAN** cell, the flexoelectric coefficients and the rotational viscosity as functions of temperature. This is a new technique in which many physical parameters can be measured simultaneously. The surface torque in a **HAN** cell has contributions from the flexoelectric, anchoring and elastic torques. On the other hand the bulk torque arises mainly from the viscous, elastic and dielectric torques. Hence a study of the electrooptical

signal from a HAN cell gives information about the relevant physical parameters.

3.1 Earlier experiments

Anchoring energy measurements are very important for a fundamental understanding of surface alignment and for device applications. There are very few accurate measurements of anchoring energy, especially its temperature dependence. Similarly there are very few measurements of the flexoelectric coefficients. We will review some of the earlier techniques used for measuring anchoring energy, rotational viscosity and flexoelectricity in this section.

One of the techniques to measure anchoring energy make use of high external fields. Fredrickz transition is a well known field induced instability in nematics. When a field (electric or magnetic field) is applied normal to a uniformly aligned director in a cell with strong anchoring, a director distortion takes place above a threshold external field, to a configuration of lower free energy. This transition in a nematic cell from a spatially uniform to a nonuniform state as a function of external magnetic or electric field is known as Freederickz transition.

Yokoyama etal [15, 16] could estimate the anchoring energy for homogeneous alignment using a high field extrapolation technique. Far above the Freederickz threshold the director is practically along the applied field except near a thin layer close to the surface. A strong torque is produced on the director at the surface. The optical phase difference ($\Delta\phi$) as well as the capacitance(C) of the cell are measured as functions of the applied voltage(V) well above the Freederickz threshold. Then the extrapolation length L is derived from the following relation [16].

$$\frac{\Delta\phi}{\Delta\phi_0} = \frac{I_0}{CV} - \frac{2L}{d}, \quad (3.1)$$

where d is the cell thickness, I_0 is a constant depending on the material parameters

and $\Delta\phi_o$ is the phase difference between the ordinary and extraordinary rays at $V=0$ and is given by

$$\Delta\phi_o = \frac{2\pi d(n_e - n_o)}{\lambda} \quad (3.2)$$

n_e and n_o are the refractive indices for the extraordinary ray and the ordinary ray respectively. λ is the wavelength of the incident beam. Hence by plotting $A^4 / \Delta\phi_o$ against $1/CV$, a straight line is obtained. L is deduced from the intercept of the straight line with the ordinate axis. Therefore the anchoring energy W can be determined by using the relation

$$W = \frac{K_{11}}{L} \quad (3.3)$$

where K_{11} is the splay elastic constant. This method involves capacitance measurements and it senses the total area of the cell. The nonuniformities in the alignment in the whole area of the cell coated with polyimide and rubbed, will give rise to errors in the measurement. Hence temperature dependent measurements using this technique [17] for polyimide coated surfaces do not produce very smooth variations.

The viscous behaviour of nematic liquid crystals can be described by five independent viscosity coefficients which are known as the Leslie coefficients. The most important combination of the Leslie coefficients is the rotational viscosity γ_1 . It is an important parameter for many electrooptical applications employing liquid crystals, because the response time of the LC device is linearly proportional to γ_1 . Several experimental methods have been developed to measure rotational viscosity [18, 19, 20]. A simple method is based on the dynamics of the Freederickz transition in the twist geometry. It is a relaxation method in which the time constant of the relaxation process from a non-equilibrium alignment of the director to the equilibrium alignment is measured. For pure twist distortion, the relaxation time τ_d

is given by the formula [21]

$$\tau_d = \frac{\gamma_1 d^2}{K_{22} \pi^2} \quad (3.4)$$

where K_{22} the twist elastic constant and d the cell thickness. However using this method it is difficult to measure γ_1 for geometries other than the twist one as determination of γ_1 is influenced by backflow effects. Another method for measuring γ_1 is by using rotating magnetic fields. γ_1 is determined by the measurement of the torque exerted on the sample rotating in a magnetic field of fixed direction. This method gives comparatively precise values. However the evaluation of the viscosity coefficient is not straightforward and this method can only be used for nematic liquid crystals with positive anisotropy of the magnetic susceptibility.

The flexoelectric coefficient ($e_1 + e_3$) has been measured earlier using a few different techniques [22, 23, 24, 25]. ($e_1 + e_3$) mainly arises from the quadrupolar densities in the medium and hence in some of these techniques an electric field gradient is used to reorient the quadrupoles. The interdigitated electrode technique devised by Marcerou and Prost [22] measures the intensity of light scattering produced by a spatially periodic distortion in the director field due to the flexoelectric effect. As an AC field is used in the experiments, this technique is quite accurate and has been used to measure ($e_1 + e_3$) as a function of temperature. However, it does not allow a determination of the sign of ($e_1 + e_3$). A pyroelectric technique has been devised by Beresnev et al [23] to measure the temperature variation of ($e_1 + e_3$) of MBBA, but its sign has not been mentioned. A DC field gradient has been used in a technique devised by Dozov et al [24, 26], but the liquid crystals usually contain ionic impurities which give rise to a double layer formation near the electrodes. As a result the electric field is partially screened and more seriously strong field gradients arise due to a non uniform ion distribution in the cell. Hence the DC measurements are not accurate enough to measure ($e_1 + e_3$) as a function of temperature.

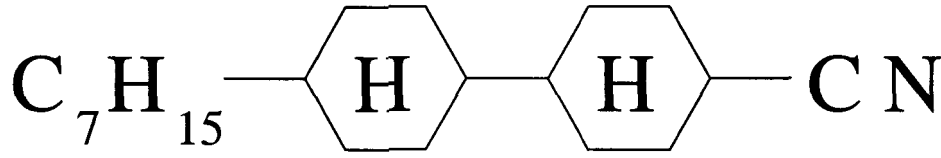


Fig. 3.1: trans-1-heptyl-4-(4-cyanocyclohexyl)cyclo hexane [CCH-7]

The flexoelectric energy density depends linearly on the curvature of the director field. As such in a sandwich cell with a planar distortion of the director field subjected to a uniform electric field, the flexoelectric coefficient does not contribute to the bulk torque (see equation 2.28). If the surface anchoring is weak the flexoelectric coupling gives rise to a surface torque which in turn produces a distortion of the director field in the cell and hence an electrooptic response [27]. Maheshwara Murthy et al [25] have demonstrated that a hybrid aligned nematic(HAN) cell produces an AC electrooptic response due to the flexoelectric effect. However they used a highly simplified model assuming a uniform field and one elastic constant approximation to analyse the response and could reproduce only the qualitative features of the experimental results.

In the previous chapter we described a numerical technique to analyse the response of such a cell quantitatively without making the approximations mentioned above. This allows us to measure the flexoelectric coefficient ($e_1 + e_3$) accurately and also to determine its sign. Further the analysis allows for a measurement of the anchoring energies at both the surfaces and the rotational viscosity coefficient.

We have conducted experiments on the electrooptic response of trans-1-heptyl-4-(4-cyanocyclohexyl)cyclo hexane(CCH-7) (see Fig. 3.1) as a function of temperature and using the numerical analysis, we have measured the temperature dependences of all the physical parameters mentioned above.

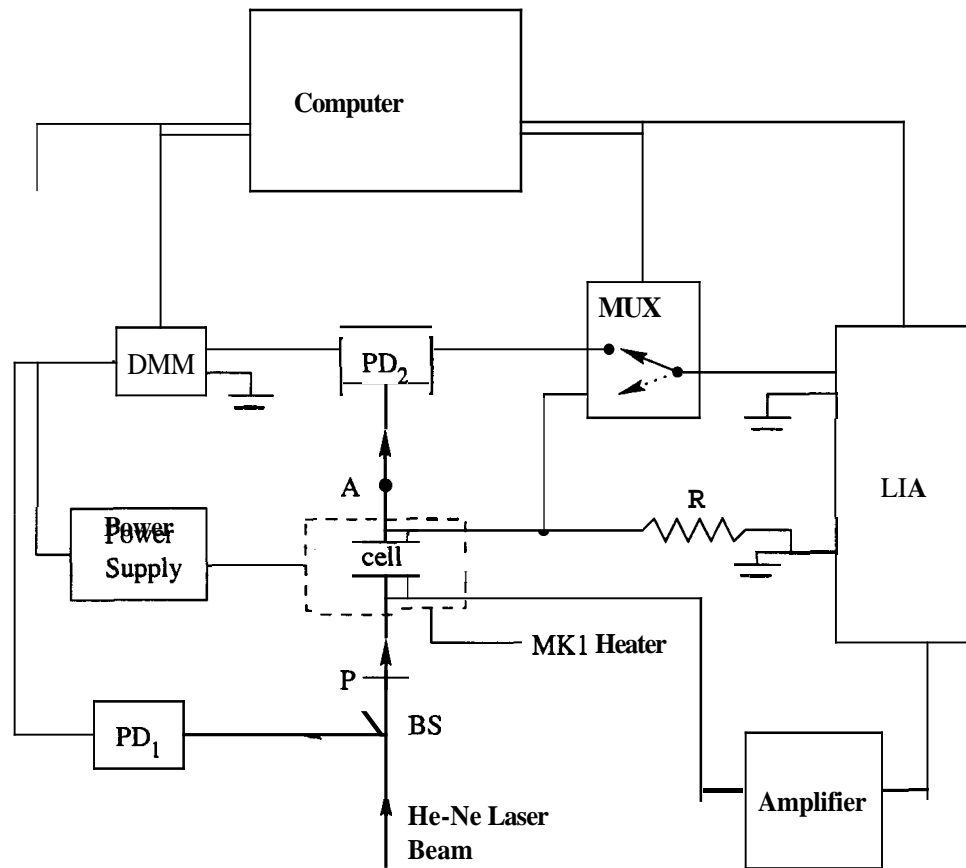


Fig. 3.2: Block diagram of the experimental setup for electrooptic measurements.

3.2 Experimental technique

The block diagram of the experimental setup is shown in Fig. 3.2. The cell is constructed using two ITO coated glass plates. One of the glass plates is treated with polyimide and rubbed for homogeneous alignment and the other plate is treated with ODSE (octadecyl triethoxy silane) for homeotropic alignment. The thickness of the cell is measured using channel spectrum as described in section 1.12 and is around $6.6\mu\text{m}$. The sample (CCH-7) has been obtained from E.Merck with the transition temperatures $K-71^{\circ}\text{C}-N-83^{\circ}\text{C}-I$. The nematic can be supercooled by approximately 15°C . The cell is filled with the compound in the isotropic phase and placed in an HS1 hot stage which is mounted on the stage of a Leitz polarising microscope. The

temperature of the sample is controlled using an Instec MK1 temperature controller. The temperature stability is better than 10mK. A platinum resistance thermometer placed close to the sample is used to measure the sample temperature accurately. In the HAN cell, two types of domains with opposite curvatures of the director can occur with equal probability as shown in Fig. 2.4. We found that by cooling the sample slowly in an electric field to the nematic phase and by reducing the field slowly we could get a single domain. The alignment is found to be quite good.

A He-Ne laser beam of low intensity is incident on a beam splitter(BS). The partially reflected light is monitored using a photodiode assembly (PD_1) for any fluctuations in the incident intensity. The transmitted light beam is monitored using a PIN photo diode and the output is fed to an operational amplifier . The photo diode assembly(PD_2) includes both the PIN diode and the opamp. The built in oscillator output of the lock-in amplifier is fed into a TREK amplifier and the amplified voltage is applied to the cell. The output of the photodiode is preamplified and connected to an HP multimeter (Model 3457A) to measure the DC component of the optical signal and to a PAR (Model 5302) lock-in amplifier to measure the AC component of the optical signal. To make conductivity measurements on the sample the lock-in amplifier can be connected to the resistor R connected in series with the sample and the voltage drop across the resistor is measured. The optical and the conductivity signals are measured alternately. Both these signals are fed to the LIA input via a multiplexer (MUX), which can be programmed to switch between these two measurement modes. The whole experimental setup is computer controlled through a Keithley interfacing card.

Initially the polariser is set parallel to the analyser. The microscope stage is rotated so that the plane containing the director is also parallel to the polariser. The incident intensity I_0 of the laser beam is then measured using the multimeter.

Then the polariser is crossed with respect to the analyser. The microscope stage is rotated so that the plane in which the director is aligned makes an angle of 45° with the crossed polarisers. In this setting the DC component and the amplitude as well as the phase of the AC component of the optical signal are measured as functions of voltage at different temperatures. The DC dark current is measured with the shutter closed both at the beginning and at the end of the experimental run. The TREK amplifier is calibrated using the same setup by connecting a resistance R_1 in the place of the cell. The amplitude (V_o) and phase (ϕ) of the output of the TREK amplifier are calculated by measuring the AC signal developed across the resistance R ($\sim 100 \Omega$) in series with a resistance $R_1 \sim 4.5k \Omega$. They are given by

$$V_o = V_2 \frac{R_1 + R}{R} \quad (3.5)$$

and

$$\phi = \phi_2 \quad (3.6)$$

where V_2 and ϕ_2 are the amplitude and phase of the signal measured across the series resistor R . An impedance analysis of the circuit is used to make the conductivity measurements of the sample as described in the next section.

3.3 Conductivity measurement.

To calculate the conductivity of the liquid crystal cell, we measure the resistance of the cell. Liquid crystals have finite resistance as they are not free of ionic impurities. A liquid crystal cell can be considered to be a capacitance (C_s) and a resistance (R_s) in parallel (see Figure 3.3). We measure the amplitude (V_m) and phase (ϕ_m) of the voltage developed across a series resistor R using a lock-in amplifier. The impedance of the sample cell is given by

$$Z_s = \frac{R_s}{(1 + i\omega C_s R_s)} \quad (3.7)$$

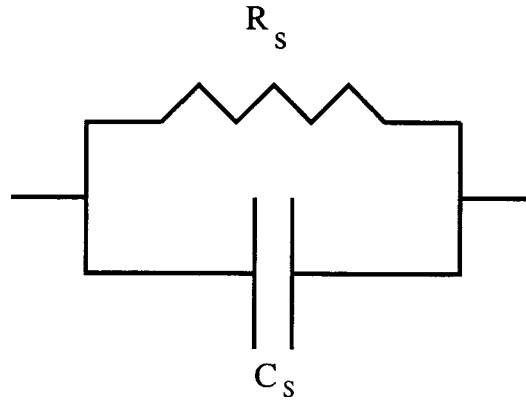


Fig. 3.3: Schematic diagram of the electrical equivalent of the experimental cell.

where R , is the resistance and C_s is the capacitance of the cell. $w = 2\pi\mathbf{f}$ where \mathbf{f} is the frequency of the applied voltage. The total impedance of the circuit (Z_t) is given by

$$Z_t = Z_s + R \quad (3.8)$$

The total current I_t , is given by

$$I_t = \frac{V_o e^{i(\omega t + \phi)}}{Z_t} \quad (3.9)$$

where V_o and ϕ are the amplitude and phase of the voltage at the output of the TREK amplifier (see section 3.2). The voltage drop across R which is measured by the LIA is given by

$$V = V_m e^{i(\omega t + \phi_m)} = I_t R \quad (3.10)$$

where V_m and ϕ_m are the amplitude and phase of the measured voltage across the series resistor R .

$$V = \frac{V_o R (\cos \phi + i \sin \phi) (1 + i\omega C_s R_s)}{R + R_s + i\omega C_s R_s R} \quad (3.11)$$

$$V_m = |V| \quad (3.12)$$

$$\tan \phi_m = \frac{ImV}{ReV} \quad (3.13)$$

Let

$$X = \frac{R + R_s + \omega^2 C_s^2 R_s^2 R}{\omega C_s R_s^2}, \quad (3.14)$$

Chapter 3

$$Y = \frac{V_m}{V_o R \sqrt{1 + X^2}}, \quad (3.15)$$

$$Z = \frac{R}{\frac{1}{XY} - R}. \quad (3.16)$$

It can be shown that

$$X = \frac{\cos \phi + \sin \phi \tan \phi_m}{\cos \phi \tan \phi_m - \sin \phi}. \quad (3.17)$$

As ϕ (the phase difference introduced by the amplifier) and ϕ_m (phase of the measured voltage across the series resistor R) are known X, Y and Z can be calculated. Simplifying the above expressions it can be shown that the sample resistance (R_s) and capacitance (C_s) are given by:

$$R_s = \frac{X}{Y(X^2 - Z)} - R, \quad (3.18)$$

$$C_s = \frac{1}{\omega R_s} \left\{ \frac{R_t(1 - R_t XY)}{R(RXY - 1)} \right\}^{0.5} \quad (3.19)$$

where $R_t = R + R_s$.

The conductivity of the sample is given by

$$\sigma_s = \frac{d}{R_s A} \quad (3.20)$$

where A is the area of the conducting region of the cell in which the sample is filled and d is the cell thickness. The area of the conducting region is obtained by measuring the empty cell capacitance. The conductivity has to be measured on the HAN cell as it can change for each individual cell. At high voltages the HAN cell is more or less homeotropically aligned. Hence the conductivity of the cell measured at high voltages can be taken as σ_{\parallel} . At lower voltages both σ_{\parallel} and σ_{\perp} contribute to the measured conductivity (a.). By assuming a director profile, σ_{\perp} can be calculated. The detailed calculation will be shown later. We will describe the electrooptic results on the compound CCH-7 in the coming section.

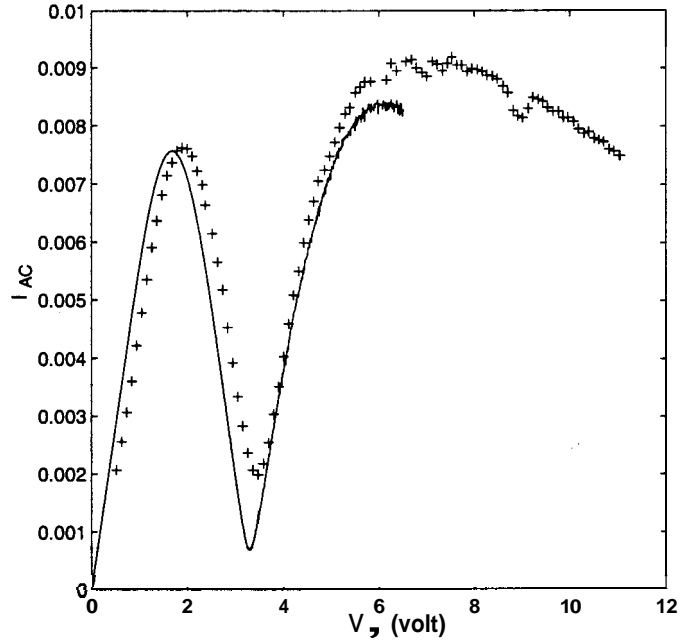


Fig. 3.4: Transmitted AC intensity coefficient I_{AC} (normalised with respect to I_0) as a function of voltage of a HAN cell with CCH-7 at $T=333.65^\circ\text{K}$. The '+' symbols indicate the experimental data. The continuous curve shows the theoretical fit in the case of an insulating nematic for $W_l=0.0241$ ergs/cm², $W_u=0.026$ ergs/cm², $e_1+e_3=8.0\times 10^{-04}$ cgs units and $\gamma_1=0.9$ poise.

3.4 Experimental results

Typical data of the transmitted AC and DC intensities normalised with respect to the incident intensity I_0 , which is corrected for the dark current (~ 0.01 volt) are shown in Fig. 3.4 and 3.5 respectively. All the measurements were made at the frequency $f=87\text{Hz}$. The f signal (Fig. 3.4) exhibits a relatively sharp maximum, a minimum and a second broad maximum as the voltage is increased. From Fig. 3.5, it can be seen that the DC signal decreases monotonically with voltage.

In chapter 2, we have derived the relevant equations to calculate AC and DC transmitted intensity profiles. The data on K_{11} , K_{33} , ϵ_\perp and $\Delta\epsilon$ for CCH-7 have been measured earlier and is shown in Fig. 3.6 and 3.7 (taken from Ref.[28]) and are used in our calculations. The data on the extra ordinary and ordinary refractive indices n_e

Chapter 3

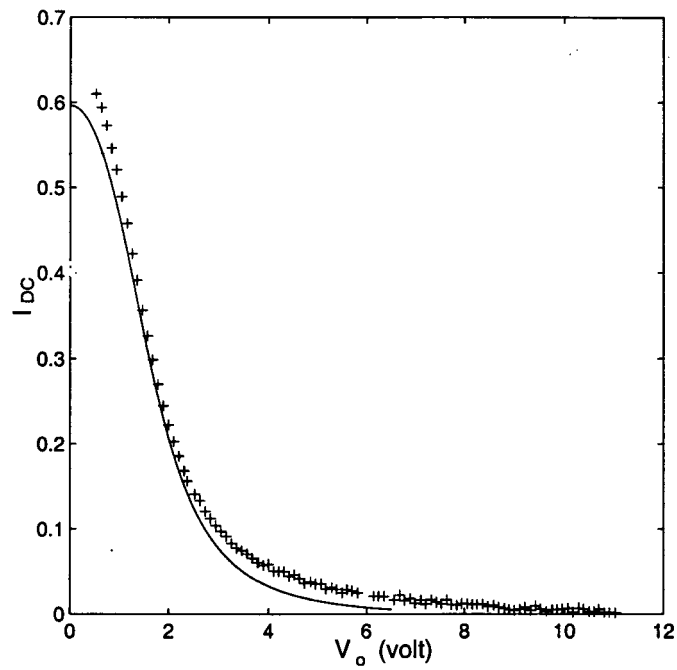


Fig. 3.5: Transmitted DC intensity coefficient I_{DC} as a function of voltage for the cell described in Fig. 3.4 at $T=333.65^{\circ}\text{K}$. The '+' symbols indicate the experimental data. The continuous curve shows the theoretical fit. The parameters are the same as in Fig. 3.4.

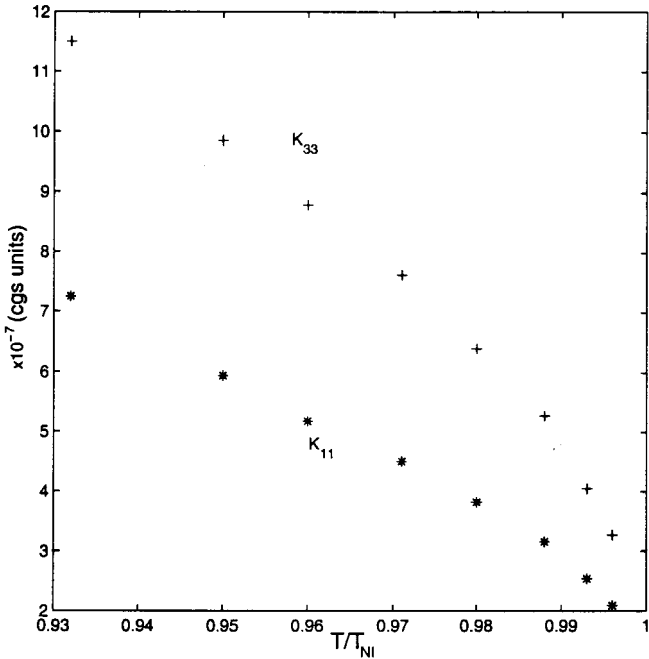


Fig. 3.6: The elastic constants K_{11} and K_{33} as functions of reduced temperature T/T_{NI} for the compound CCH-7 taken from the paper by Schad [28].

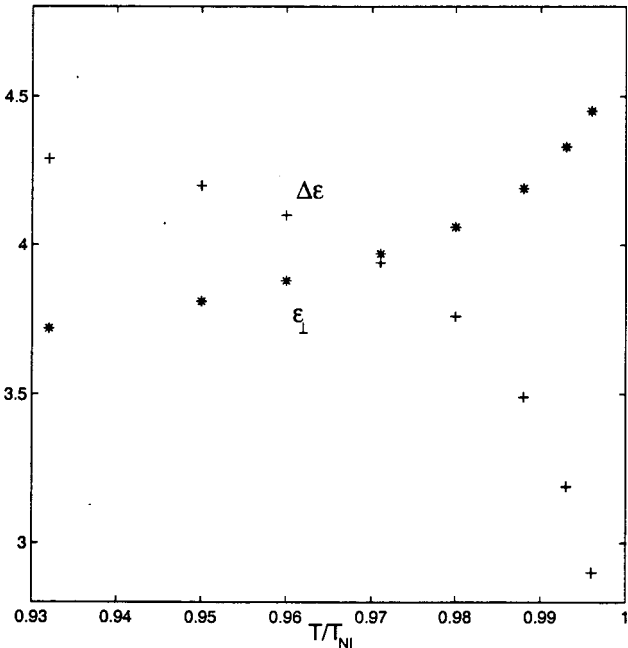


Fig. 3.7: The dielectric constants $\Delta\epsilon$ and ϵ_{\perp} as functions of reduced temperature T/T_{NI} for the compound CCH-7 taken from the paper by Schad [28].

Chapter 3

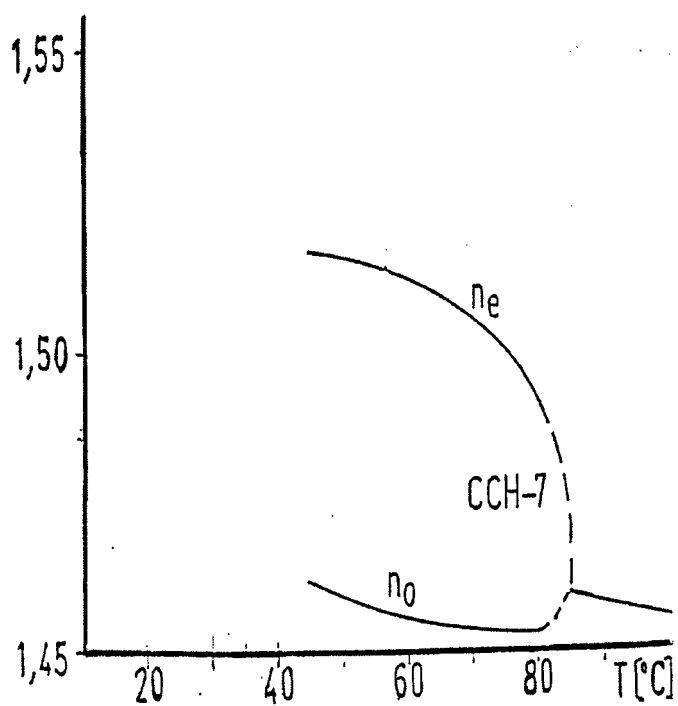


Fig. 3.8: The refractive indices n_e and n_o as functions of temperature T for the compound CCH-7 taken from the paper by Pohl [14].

and n_o are available in literature and is shown in Fig. 3.8(taken from Ref. [14]). By assuming some reasonable initial values of W_l , W_u , $(e_1 + e_3)$ and γ_1 the transmitted intensity profiles are calculated. The data is computed by assuming the nematic to be an insulator. Initially the values of W_l , W_u , $(e_1 + e_3)$ and γ_1 were adjusted by hand to get a qualitative agreement between the calculated profile and the experimental one at 60°C. Later a minimisation routine Amoeba [13] was modified and used for adjusting the parameters. The calculated AC and DC transmission coefficients are compared with the experimental data in Fig. 3.4 and 3.5 respectively. The fitting procedure was simpler for the other temperatures as we could make a better guess of the initial values using the parameters of the previous fit at a nearby temperature. The calculated phase of the optical signal reverses sign with that of $(e_1 + e_3)$. By comparing the calculated phase of the AC signal with the experimentally measured value, the sign of $(e_1 + e_3)$ was determined to be positive for CCH-7.

In chapter 2, we have derived the equations for the transmitted intensity profiles of a conducting nematic also. As in the case of an insulating nematic, the values of K_{11} , K_{33} , ϵ_{\perp} , $\Delta\epsilon$, n_e and n_o are used from earlier measurements [14, 28]. In addition to these parameters there are two more parameters involved in these equations namely σ_{\perp} and A_a . As mentioned in section 3.3, the conductivity of the cell measured at high voltages can be taken as σ_{\parallel} ($\sigma_{\parallel} = 6.3 \times 10^{-8} \text{ ohm}^{-1} \text{ cm}^{-1}$ (567 cgs units) at 60°C). At lower voltages both σ_{\parallel} and σ_{\perp} contribute to the measured conductivity. The conductivity σ_s , measured across the cell is given by

$$\sigma_s = \frac{\int_{\theta_l}^{\theta_u} (\sigma_{\parallel} \cos^2 \theta + \sigma_{\perp} \sin^2 \theta) d\theta}{\int_{\theta_l}^{\theta_u} d\theta} \quad (3.21)$$

where l and u refer to the lower and upper surfaces respectively. Using the above equation and from the director profile obtained in the case of an insulating nematic, σ_{\perp} and hence $\Delta\sigma$ can be calculated. σ_{\perp} was found to be $4.77 \times 10^{-8} \text{ ohm}^{-1} \text{ cm}^{-1}$ (430

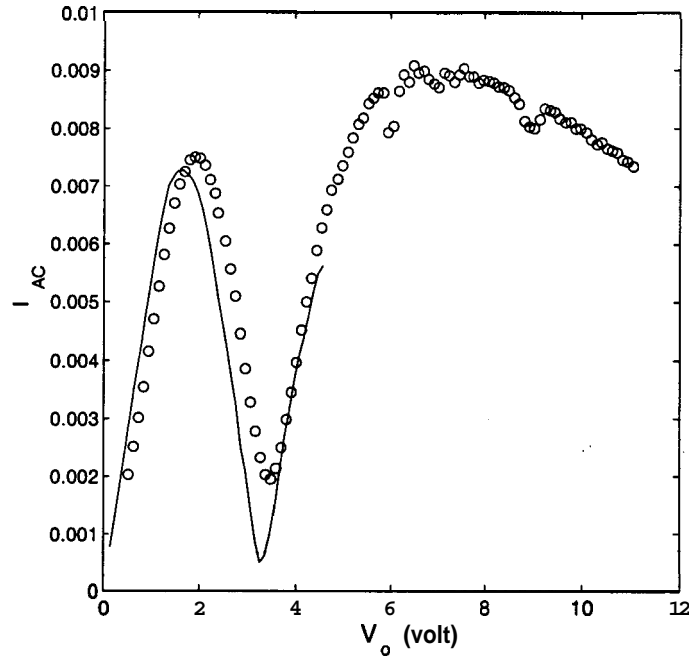


Fig. 3.9: Transmitted AC intensity coefficient I_{AC} (normalised with respect to I_0) as a function of voltage at $T=333.65^\circ\text{K}$. The 'o' symbols indicate the experimental data. The continuous curve shows the theoretical curve for a conducting nematic for $W_l=0.0241$ ergs/cm², $W_u=0.026$ ergs/cm², $e_1+e_3=8.0\times 10^{-04}$ cgs units and $\gamma_1=0.9$ poise.

cgs units) at 60°C . The calculations for the conducting nematic are computationally more involved than in the case of an insulating nematic and we could not implement the fitting procedure. The set of values of W_l , W_u , (e_1+e_3) and γ_1 which was needed to obtain the best fit in the case of an insulating medium, has been tried for the conducting case also. In the case of a conducting nematic the calculated AC and DC transmitted intensities for a conducting nematic are shown in Fig. 3.9 and 3.10. The fit is similar to that obtained for an insulating nematic (see Fig. 3.4 and 3.5). As the fit is not optimised, the root mean square deviation is slightly larger (2.5×10^{-4}) compared to that obtained for an insulating nematic (1.5×10^{-4}). We could not extend the calculations beyond 4.8 volts as they involved too much computation. All further discussion is for the fitted values obtained for an insulating sample.

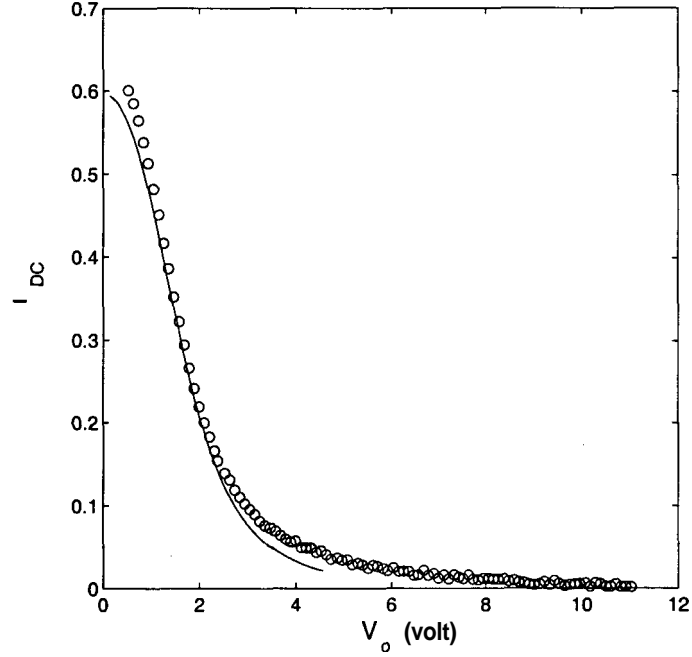


Fig. 3.10: Transmitted DC intensity coefficient I_{DC} as a function of voltage at $T=333.65^\circ\text{K}$. The '+' symbols indicate the experimental data. The continuous curve shows the theoretical curve. The parameters are the same as in Fig. 3.9.

The flexoelectric coupling is linear with the applied electric field as well as the curvature of the director field. The flexoelectric torque at the surface is proportional to $\sin(2\theta)$. Hence θ should have a value other than 0 or $\frac{\pi}{2}$ to produce a flexoelectric surface torque. At 60°C $W_l=0.024$ ergs/cm² and $W_u=0.026$ ergs/cm² are comparable. We have shown the θ_o , θ_1 and θ_2 profiles in Fig. 3.11-3.16 at different voltages which correspond to first maximum, first minimum and second maximum of the electrooptic signal(see Fig. 3.4). From Fig. 3.11 we can see that θ_{ol} is considerably different from zero. θ_{ou} is lower than $\frac{\pi}{2}$. θ_1 and θ_2 have considerable values at both the surfaces (see Fig. 3.14). As a result these two surfaces give rise to the flexoelectric f signal at low fields, which being $\propto E$ (see equation 2.36) increases with the applied field. However as the field is increased further, the dielectric torque on the medium which depends quadratically on the field, reduces θ_{ol} and hence θ_{1l} and

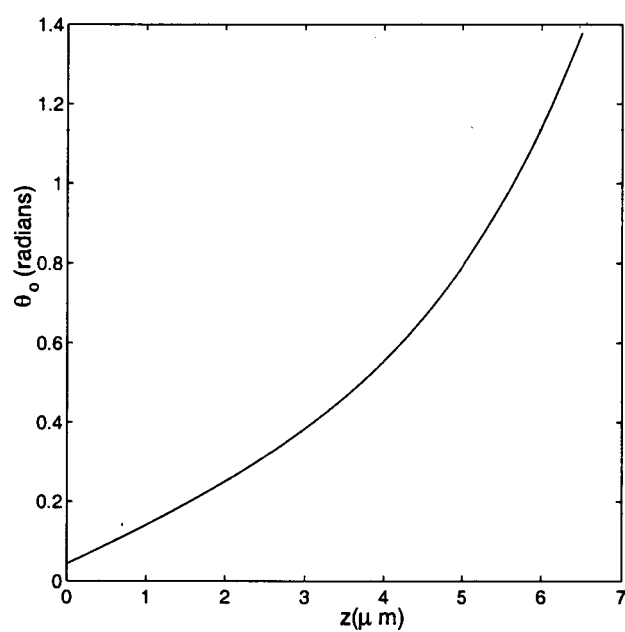


Fig. 3.11: The calculated variation of θ_0 as a function of position z at voltage $V_0=1.8$ volts corresponding to the first maximum in the calculated transmitted AC optical signal. The calculations are performed upto $z=6.6 \mu\text{m}$ which corresponds to the thickness of the cell.

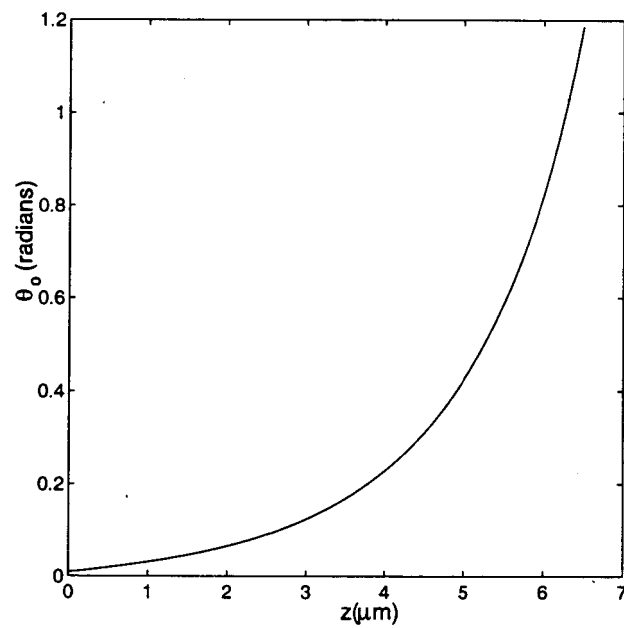


Fig. 3.12: The calculated variation of θ_0 as a function of position z at voltage $V_0=3.3$ volts corresponding to the first minimum in the calculated transmitted AC optical signal.

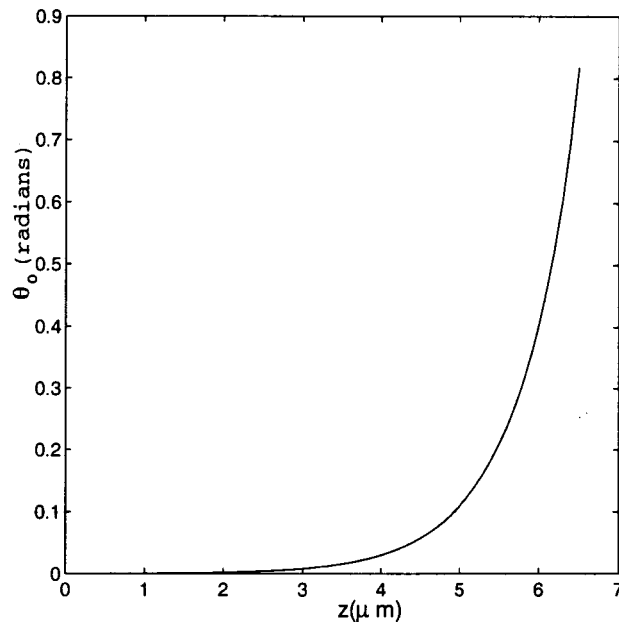


Fig. 3.13: The calculated variation of θ_0 as a function of position z at voltage $V_0=6.3$ volts corresponding to the second maximum in the calculated transmitted AC optical signal.

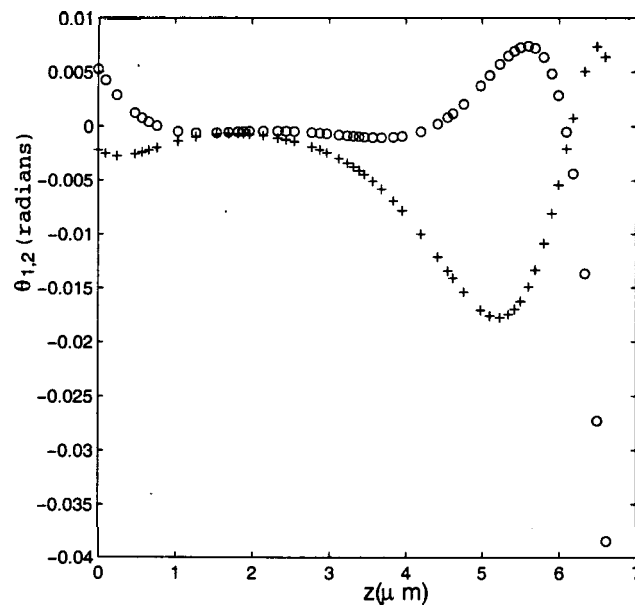


Fig. 3.14: The calculated variation of θ_1 and θ_2 as functions of position z at a voltage $V_0=1.8$ volts. The '+' symbols indicate the θ_1 profile and the 'o' symbols indicate the θ_2 profile.

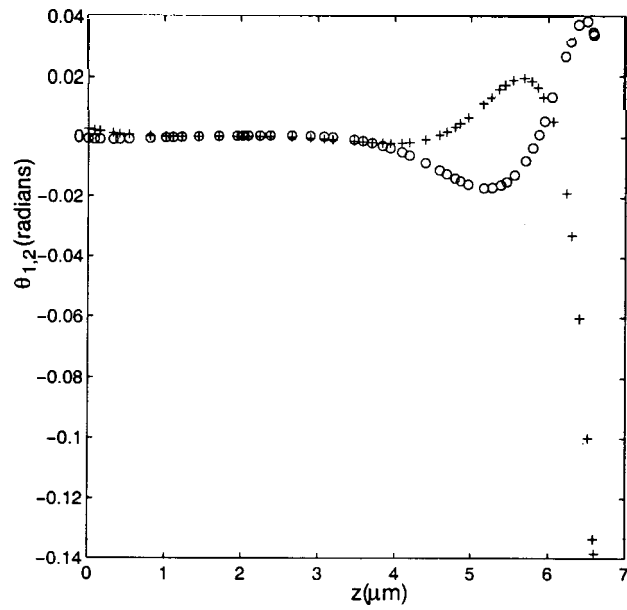


Fig. 3.15: The calculated variation of θ_1 and θ_2 as functions of position z at a voltage $V_0=3.3$ volts. The '+' symbols indicate the θ_1 profile and the 'o' symbols indicate the θ_2 profile.

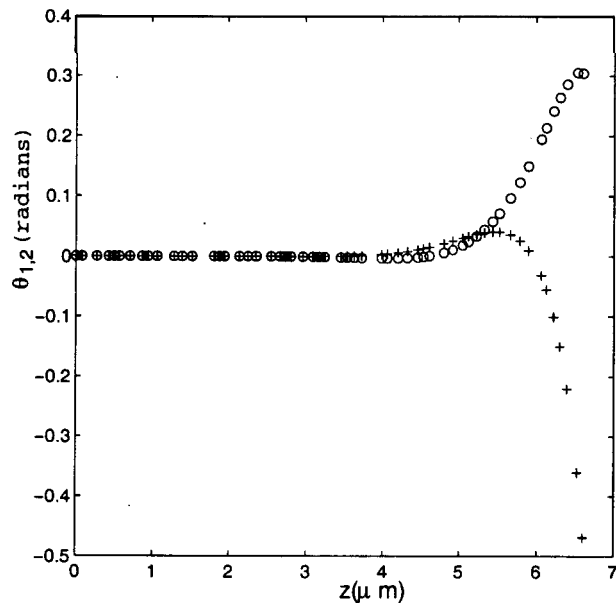


Fig. 3.16: The calculated variation of θ_1 and θ_2 as functions of position z at a voltage $V_0=6.3$ volts. The '+' symbols indicate the θ_1 profile and the 'o' symbols indicate the θ_2 profile.

θ_{2l} are also reduced (see Fig. 3.12, 3.15). Thus the flexoelectric signal from the homeotropically anchored surface ($\propto \sin(2\theta)$) is reduced. At even higher fields the dielectric torque reduces the angle θ_{ou} further from $\frac{\pi}{2}$ (see Fig. 3.13) at the homogeneously aligned surface. The curvature is now confined to a small thickness close to this surface. Hence the amplitudes of θ_1 and θ_2 (see Fig. 3.16) increase at this surface. This in turn gives rise to an increased flexoelectric torque on that surface and hence to an increase in the f signal.

We have conducted independent experiments in the homogeneous geometry with both the plates of the cell treated with polyimide and rubbed, in order to check whether the values of W_u (~ 0.026 ergs/cm² at 60°C) are reasonable. We have measured the $\text{D}\odot$ transmission coefficient between crossed polarisers set at 45° to the undistorted director as a function of an applied AC voltage. We have also measured the capacitance of the cell as a function of the applied voltage. Using the high field extrapolation technique as described in the beginning of this chapter [15, 16] we could estimate that W_u corresponding to the plate treated for homogeneous alignment is $\simeq 0.04$ ergs/cm² and $\simeq 0.03$ ergs/cm² respectively in two independent cells of thickness $\simeq 7.4\mu\text{m}$ at 60°C. Considering the fact that the measurements on these cells and on the HAN cell were made using very different techniques, the similar values found for W_u are quite satisfactory. We also measured the values of W_u at a few different temperatures to find that as expected, W_u decreases with temperature. However the error in W_u is $\sim \pm 0.005$ ergs/cm² using this technique so that the data cannot be used for any quantitative interpretation of the temperature dependence. Indeed other measurements using this technique [17] appear also to point to such inaccuracies in this technique. As can be seen in Fig. 3.17, our technique gives a much smoother temperature variation pointing to a much better accuracy.

It can be seen from Fig. 3.4 and 3.5 that even the best fitting yields theoretical

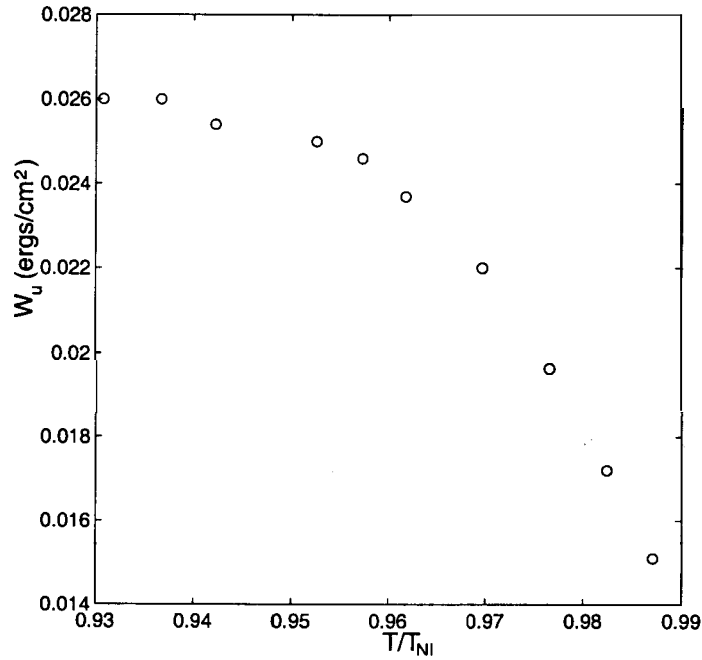


Fig. 3.17: The anchoring energy W_u as a function of reduced temperature T/T_{NI} .

variations of the AC and DC electrooptic signals which systematically occur at a slightly lower voltage compared to the experimental data. This systematic deviation might have resulted from the assumption of an insulating nematic. We can estimate the errors in the calculated values due to those in the assumed parameters. The stated error in the measurements of K_{11} and K_{33} is $\pm 4\%$, but varying K_{11} and K_{33} by these limits does not change the quality of the fit or the values of the four fit parameters perceptibly. Similarly, the small error in the dielectric data ($\sim \pm 0.2\%$) also does not affect the results. The errors in n_e and n_o are not stated by the authors [14]. If we assume that the error in each is ± 0.001 which is typical for such measurements, the main effect is on the parameter W_l and $(e_1 + e_3)$. While W_l changes by $\pm 4\%$ for a change of ± 0.001 in n_e , it changes by **72%** for a similar change in n_o . Hence the overall error due to the errors in the assumed parameters is only $\pm 6\%$ in W_l . $(e_1 + e_3)$ changes by $\pm 2.5\%$ due to an error of ∓ 0.001 in n_e

and ± 0.001 in n_o , so that the overall error in $(e_1 + e_3)$ is about $\pm 5\%$. The other fit parameters are insensitive to the errors in n_e and n_o .

We have performed the calculations only upto 6.5 volts as the magnitudes of θ_1 and θ_2 cannot be considered small for higher voltages. The linearisation of θ_t is not a good approximation at higher voltages. The numerical error also becomes large as voltage becomes high as can be seen in Fig. 3.4. Moreover the backflow effects can no longer be ignored when the value of θ_t becomes significant. Indeed as we have forced the linearisation approximation upto 6.5 volts, part of the systematic deviation referred to earlier may be caused by the inadequacy of this assumption at higher voltages.

We found that beyond 79°C the theoretical calculations do not agree well with the experimental data. Hence we have not shown the calculated values beyond this temperature. The main reason for this problem is the assumption of an insulating medium, which is a reasonable approximation at lower temperatures but is inadequate at higher temperatures.

It is well known that the surface properties of a nematic can be indeed very complex. For example, the nematic can have a surface polarisation near the homeotropically aligned surface [29]. Similarly any electrical polarisation due to adsorbed ions, etc can also effectively change the surface properties [30]. We have no explicit information on these phenomena in the present case, and there is no simple way of including these effects in the calculations. As such, we have taken the simple approach of a) assuming that $(e_1 + e_s)$ has the same value at both the surfaces and b) all other processes effectively change the values of W_l and W_u so that the measurements yield only 'dressed' or effective values of the anchoring energies at the two surfaces. This approximation maybe partly responsible for the systematic error in the fitting shown in Fig. 3.4 and 3.5. However this simplified assumption appears

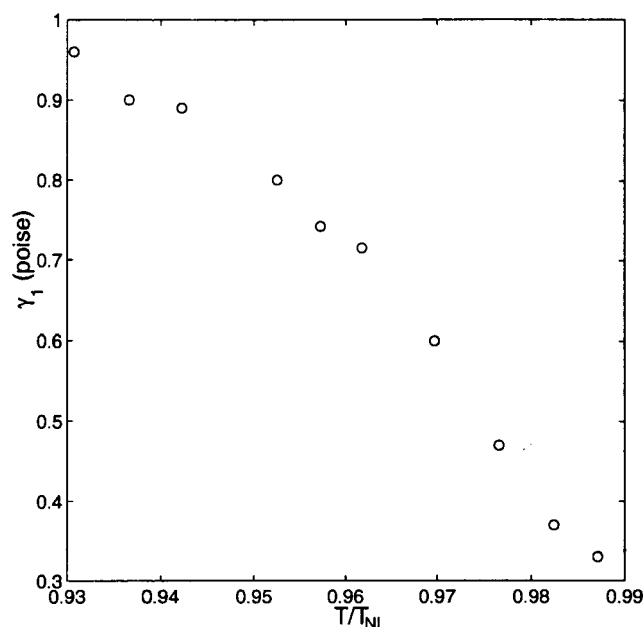


Fig. 3.18: Variation of the rotational viscosity coefficient (γ_1 in poise) as a function of the reduced temperature T/T_{NI} .

to be justified, in view of the results to be discussed in the next section in which we find that the temperature variations of all the parameters can be understood physically.

3.5 Results and discussion

The variation of γ_1 as a function of reduced temperature T/T_{NI} and the variation of the natural logarithm of γ_1 with $(1/T)$ are shown in Fig. 3.18 and 3.19 respectively. The slope of the curve increases rapidly as the temperature increases. A similar trend has been seen in other compounds [19]. γ_1 measures the rotational viscosity of the director. As has been discussed theoretically by several authors [31, 18] the orientational order has a direct influence on γ_1 apart from the usual temperature dependence of viscosities. This leads to the nonlinear variation seen in Fig. 3.19.

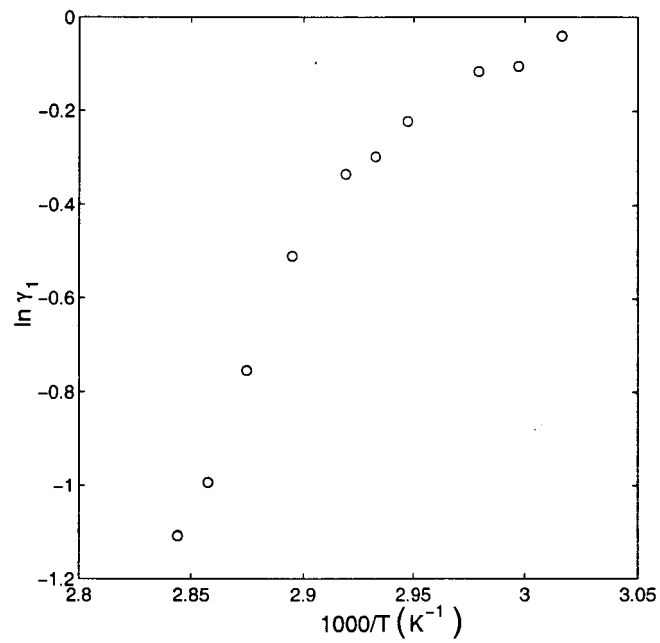


Fig. 3.19: Variation of the natural logarithm of the rotational viscosity coefficient (γ_1 in poise) as a function of the reciprocal of temperature (in K).

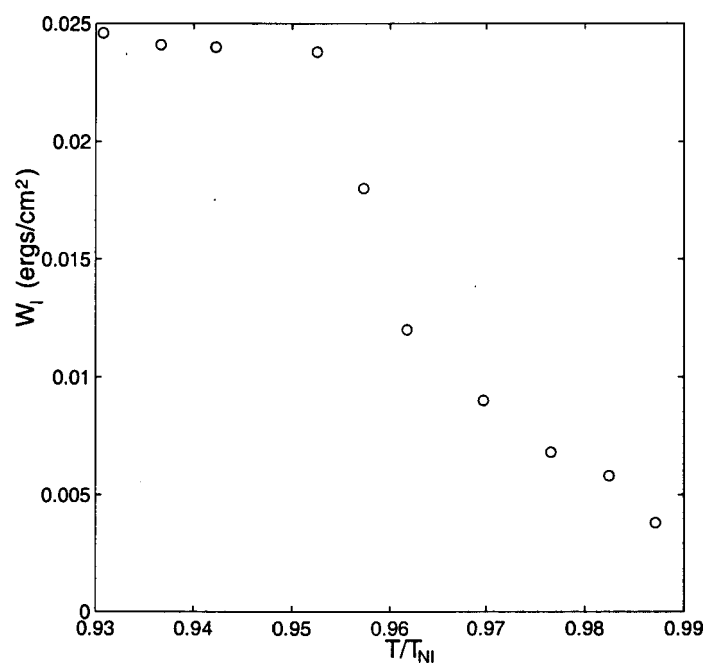


Fig. 3.20: The anchoring energy W_l as a function of reduced temperature T/T_{NI} .

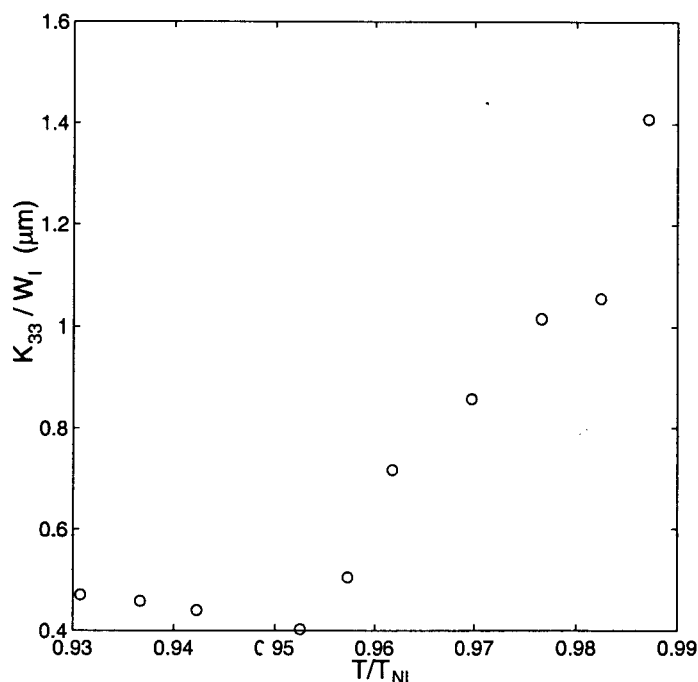


Fig. 3.21: Variation of the extrapolation length at the homeotropically aligned surface as a function of reduced temperature T/T_{NI} .

The anchoring energy of the homeotropic surface is shown as a function of reduced temperature in Fig. 3.20. The curvature elastic constants (K_{ii}) as well as the anchoring energy (W) vary as S^2 in the mean field approximation. Hence the extrapolation length (L) which is defined as K_{ii}/W [1] should be independent of temperature. For the homeotropic surface $L_l = K_{33}/W_l$. It is shown in Fig. 3.21 as a function of the reduced temperature. K_{33} of CCH-7 varies smoothly with temperature, though not as S^2 [28]. The extrapolation length shows a sharp increase beyond $T/T_{NI} = 0.95$ which arises from the trend in W_l . The sharp increase of L_l means that the anchoring potential has a shallower minimum as a function of the polar angle θ above this temperature. The homeotropic anchoring is obtained because of the steric interaction between the CCH-7 molecules and the ODSE layer which consists of chains with 18 carbon atoms. $T/T_{NI} = 0.95$ corresponds to 66°C

and it is known that the polyethylene chains soften around this temperature. Hence we attribute the weakening of W_l to the conformational degrees of freedom of ODSE chains which increase above this temperature.

The ODSE chains are anchored to the glass surface, and we can expect that the orientational order parameter of the chain segments near the tips decrease initially, and as the temperature is increased, the disorder of chains progressively increases. A similar phenomenon is known to occur in the end chains of nematogenic molecules [32]. To describe this '2D-phase transition' like behaviour we assume that the relative increase in L_l viz, $(L_l - L_{l0})/L_{l0}$ in which L_{l0} is the background value in the absence of the transition, can be treated as a 'disorder' parameter. By definition, this parameter ≥ 0 , and in analogy with the Landau theory we can write a phenomenological expression for the free energy density due to disorder as

$$F = \frac{a}{2} \left(\frac{L_l - L_{l0}}{L_{l0}} \right)^2 + \frac{b}{4} \left(\frac{L_l - L_{l0}}{L_{l0}} \right)^4 \quad (3.22)$$

where $a = \alpha(T_f - T)$. Minimising the free energy with respect to the disorder parameter, the latter varies for $T > T_f$ as

$$\frac{L_l - L_{l0}}{L_{l0}} = \frac{\alpha}{b} (T - T_f)^{\frac{1}{2}}. \quad (3.23)$$

The disorder parameter in the transition region can be indeed fitted to the above form with $T_f = 67.7^\circ\text{C}$ and $\alpha/b = 0.92$. As can be seen in Fig. 3.21, L_l shows a large increase at the highest temperature which is hence not used in the fitting. This increase probably arises from flexibility of the CCH-7 molecules as will be discussed later.

The anchoring energy of the homogeneous surface is shown as a function of reduced temperature in Fig. 3.17. The extrapolation length (L_u) at the homogeneously anchored surface (K_{11}/W_u) is shown as a function of reduced temperature in

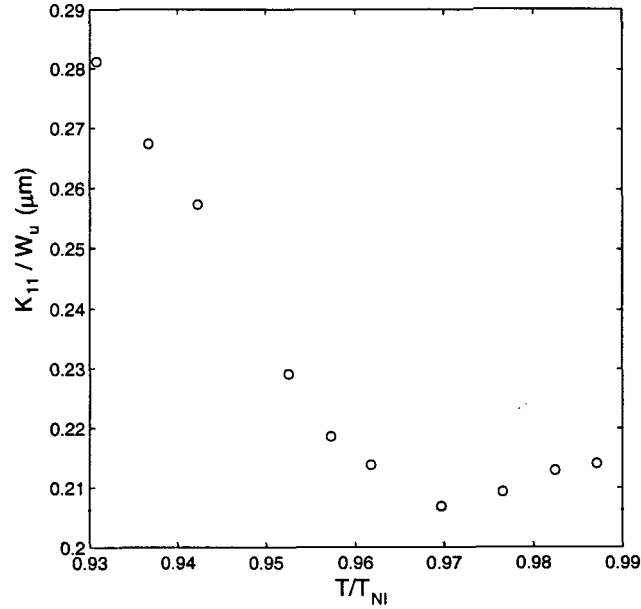


Fig. 3.22: Variation of the extrapolation length at the homogeneously aligned surface as a function of reduced temperature T/T_{NI} .

Fig. 3.22. L_u shows an unusually large decrease as the reduced temperature is raised to -0.97 . The slope of the variation of L_u changes sign beyond this temperature ($T = 72^\circ\text{C}$).

As we shall see below, the flexoelectric coefficients also show nonsmooth variations around this temperature. The main contribution to $(e_1 + e_3)$ comes from the quadrupolar effect. In such a case, $(e_1 + e_3) \propto S$ [11]. The variation of $(e_1 + e_3)$ and $(e_1 + e_3)/S$ as a function of T/T_{NI} are shown in Fig. 3.23 and 3.24 respectively. The order parameter data is taken from [33]. At low temperatures (upto 72°C) this ratio is practically independent of temperature, as expected from the quadrupolar effect. Beyond this temperature, there is a sharp decrease in $(e_1 + e_3)/S$ suggesting that the effective quadrupolar contribution is reduced. $(e_1 - e_3)/K$ of CCH-7 where K is an effective elastic constant has been measured as a function of temperature by Maheshwara Murthy et al [26]. $(e_1 - e_3)$ mainly arises from the transverse dipole

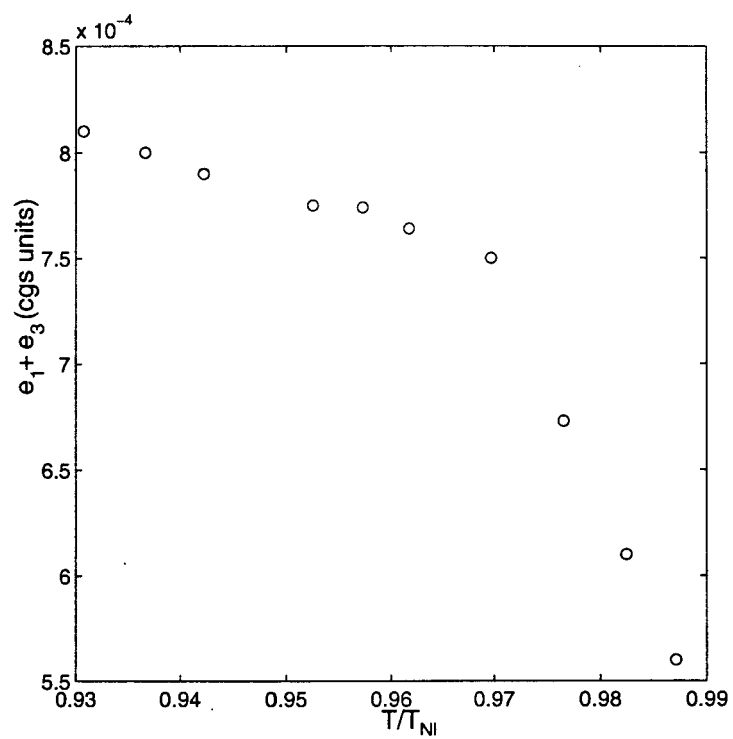


Fig. 3.23: The flexoelectric coefficient ($e_1 + e_3$) as a function of reduced temperature T/T_{NI} .

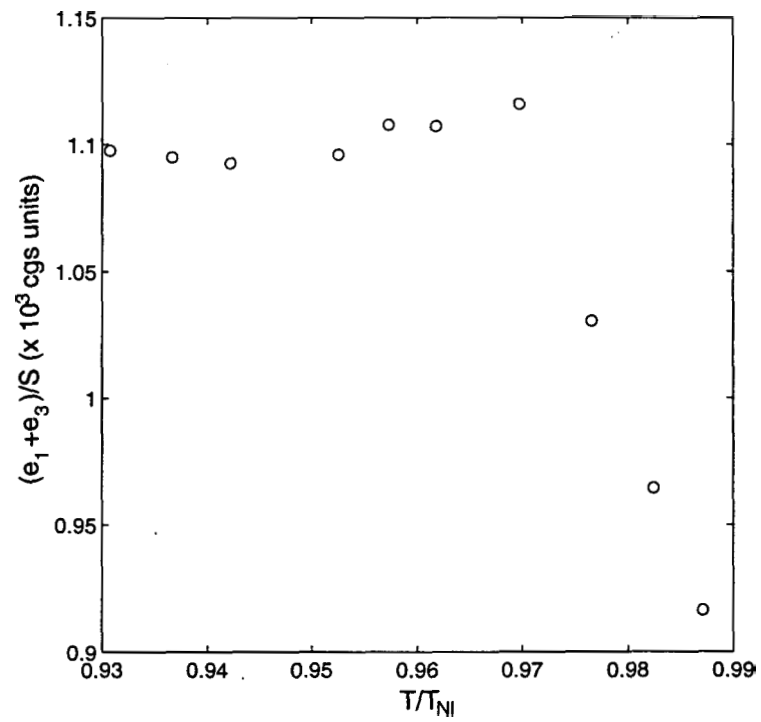


Fig. 3.24: The ratio of the flexoelectric coefficient $(e_1 + e_3)$ over the order parameter S as a function of reduced temperature T/T_{NI} .

moments of the molecules in which case $(e_1 - e_3) \propto S^2$. As such, the above ratio is expected to be essentially independent of temperature. However it was found that the magnitude of $(e_1 - e_3)/K$ which has a negative sign increased with temperature. Further, the slope of the variation itself increased at $T/T_{NI} \simeq 0.97$. The above observations indicate that there is a subtle change in the physical properties of the medium at a reduced temperature 210.97. The ratio $\Delta\chi/\Delta\epsilon$ of CCH-7 where $\Delta\chi$ is the anisotropy of diamagnetic susceptibility and $\Delta\epsilon$ the dielectric anisotropy has been measured as a function of temperature by Schad et al [28]. $\Delta\chi$ is known to be strictly proportional to the order parameter S . $\Delta\chi/\Delta\epsilon$ of CCH-7 decreases continuously as the temperature is increased. We interpret this result as follows: Due to the highly polar cyano end group, it is expected that CCH-7 molecules can exhibit antiparallel pairs [1]. As the molecules do not have any phenyl rings, the overlap between the neighbours occurs only near the polar groups. As such, this pairing is rather fragile and can easily break up as the temperature is increased. The paired molecules have a smaller effective dipole moment than the unpaired ones and hence at higher temperatures $\Delta\epsilon$ does not decrease as fast as S , due to a larger orientation polarisation. We believe that the highly polarisable polyimide surface would have stronger attractive interaction with the more strongly polar monomers than with the pairs. This could in turn produce effectively a stronger anchoring as the reduced temperature is increased to 0.97. The above mentioned antiparallel pairing between the dipoles also produces a strong quadrupole moment. It is easily verified that it can lead to the positive sign of $(e_1 + e_3)$ in CCH-7. Indeed all compounds with the cyano end group are known to have a positive $(e_1 + e_3)$ [26].

We believe that another molecular process already discussed in [26] is important for the changes occurring at the reduced temperature of 0.97. The two cyclohexane rings in a CCH-7 molecule are connected by a C-C bond, around which rotational

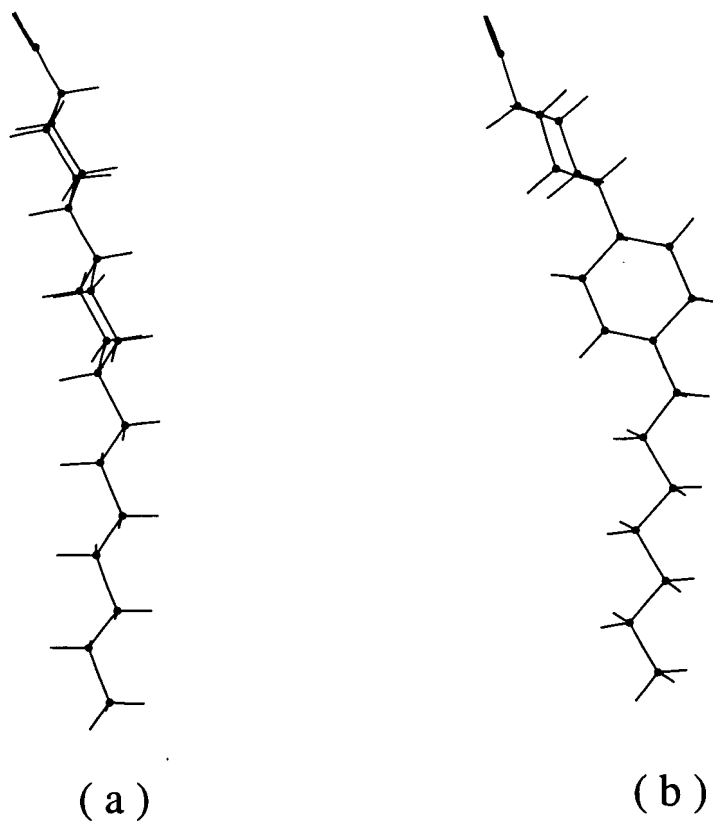


Fig. 3.25: Molecular structure of CCH-7. (a) Note that in the ground state the molecule is nearly straight. (b) A rotation about the C-C bond between the two rings produces a bent structure in CCH-7. (The structures were produced using a software which minimises the energy).

degrees of freedom can be excited especially at higher temperatures. Further, the alkyl chain of CCH-7 can also become more flexible as we discussed in the case of ODSE chains covering the lower surface.

The result is that 'bent' configurations can occur frequently at higher reduced temperatures (Fig. 3.25). These configurations can effectively reduce the anchoring energy (W_u) for homogeneous alignment beyond $T/T_{NI}=0.97$ (Fig. 3.22). The bent configuration also gives rise to a positive e_3 and hence to the negative sign of $(e_1 - e_3)$ as discussed in [26]. Indeed the magnitude of $(e_1 - e_3)/K$ increases rapidly beyond the reduced temperature of 0.97 as the relative concentration of molecules with bent configuration increases [26]. Further, such configurations effectively reduce the component of quadrupole moment along the 'long axis' of the molecule and in turn give rise to the rapid decrease of $(e_1 + e_3)/S$. We may note that L_l whose temperature dependence is dominated by the chain configuration of ODSE also shows a rapid increase at the last temperature of measurement, perhaps due to the increase in the bent configurations of CCH-7 molecules. We also note that Dozov et al [34] found evidence for a conformational contribution to flexoelectricity in the case of 8OCB.

3.6 Conclusions

A relatively simple AC electrooptic experiment conducted in a HAN cell is described in this Chapter. After a detailed numerical analysis we have been able to determine the magnitude as well as sign of $(e_1 + e_3)$ of CCH-7 as a function of temperature. In addition, we have also been able to measure the anchoring energies and the rotational viscosity coefficient as functions of temperature. The temperature dependence of the relevant extrapolation length indicates a '2D phase transition' like behaviour at the homeotropically anchored surface. We have used a simple Landau model to describe this transition and we attribute it to the conformational degrees of freedom of the

ODSE chains which take on a collective character beyond 66°C . $(e_1 + e_3)/S$ and L_u show a sharp variation at $T/T_{NI} \simeq 0.97$ which can be interpreted as arising from the flexibility of CCH-7 molecules.

As discussed earlier, the calculations have been made only upto 79°C . The conductivity of the sample becomes rather important beyond this temperature and the assumption that the nematic is an insulator is no longer appropriate.